Optical reflectivity of molten Se_xTe_{1-x} alloys

R. Fainchtein and J. C. Thompson
The University of Texas at Austin, Austin, Texas 78712
(Received 10 January 1983)

Normal reflectance of a series of molten Se_xTe_{1-x} alloys behind a sapphire window were obtained. The measurements were made for 11 alloy compositions and three temperatures, over the (0.7—5.5)-eV range. The optical data support the existence of three regimes. One is metallic, and two are semiconducting with different band gaps. Transitions between the different regimes can be achieved by changes in alloy concentration and temperature. The model presented is consistent with previously reported dc transport measurements.

I. INTRODUCTION

Molten alloys of Se with Te are among the most extensively investigated liquid semiconductors.[1,2] Perron[3] has measured the resistivity and thermoelectric power and Cutler and co-workers[4] have recently verified his results. Endo's group has studied pressure effects on the conductivity.[5] Gardner and Cutler[6] have studied the magnetic susceptibility and Rabit and Perron[7] have also determined the position of the optical-absorption edge. In addition, optical data have been published for pure Se and pure Te.[8,9] Density and structure data have been reported by Ruska[10] and by Bellissent and Tourand,[11] respectively.

The transport measurements[3] suggest that there are three different regions in the temperature-composition diagram for Se_xTe_{1-x} alloys. Each region is characterized by different values of conductivity activation energy, etc. Figure 1 shows the boundaries of these regions (I-II-III) as determined from a characteristic change in the values of a variety of parameters[3,10–13] together with the liquidus. The picture of the Se-Te alloy system is as follows. At high temperatures and high Te content (small x) the alloys are essentially metallic. This is region III of Fig. 1. As the Se fraction increases, there is a metal-semiconductor transition so that at, for example, 500 °C and 30 at. % Se, the system is semiconducting. All alloys in this range (region II of Fig. 1) have the same conductivity activation energy[3] of 1.2 eV. There is a second transition at still higher Se content and lower temperatures to an apparent semiconductor (region I of Fig. 1) with a somewhat smaller band gap (activation energy 0.8 eV). The activation energy of pure Se is 1.2 eV.[2]

Other measurements are only partially consistent with Fig. 1. The susceptibility data[6] indicate a concentration- and temperature-dependent activation energy (with some scatter) of 0.7 eV over the range $0.4 < x < 1.0$ (region I). There is no sign of the transition between regions II and III of Fig. 1. As in the conductivity, the spin density loses some of its temperature dependence at the highest temperatures in the Te-rich end of the composition range. The susceptibility χ is proportional to $\sigma^{1/2}$ in this range for $x < 0.5$. See the region marked III in Fig. 1. Such behavior is often considered charac-

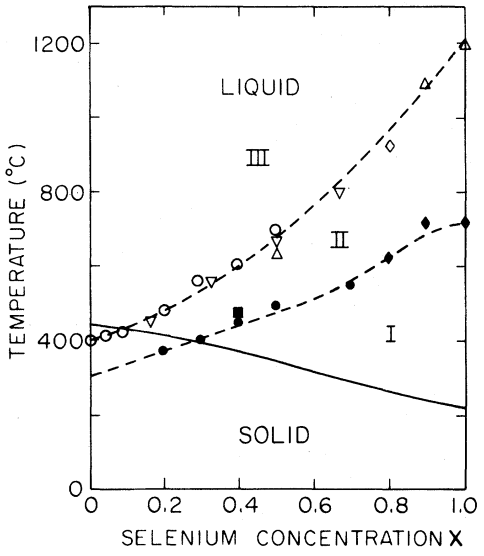

FIG. 1. Composite diagram displaying a picture of the liquid Se_xTe_{1-x} alloys. The lower solid line is the liquidus curve from Hansen (Ref. 12). The two dashed lines are drawn to guide the eye through points derived from changes in dc conductivity measurements and other parameters, ○ and ● (Ref. 3); △ [Ref. 13(a)]; ◇ and ◆ [Ref. 13(b)]; thermal expansion coefficients, ∇ [Refs. 10 and 13(a)]; and structure ■ (Ref. 11). Regions I, II, and III are defined in the text.

teristic of diffusive transport.[2,14] The slope of the χ-vs-$\sigma^{1/2}$ plot is different for pure Te than for the other alloys. Endo constructed[5] a single phase boundary in the center of region II from his pressure measurements.

There is a minimum[10,13,15] in the thermal expansion coefficient $\alpha \equiv V^{-1}(\partial V/\partial T)_p$. The locations of the minima are shown in Fig. 1 and they may be seen to correspond to the same semiconductor-to-metal transition (II to III) which is indicated by the resistivity. The density data[10] apparently give no sign of the semiconductor-semiconductor transition. Bellissent and Tourand[11] have used neutron diffraction to determine the structure factors of Se_xTe_{1-x} alloys at 475 °C. They find that the coordination number is fixed near 2 for $0.4 < x$ then rises smoothly toward 3 as x approaches zero. The rise toward threefold coordination begins abruptly at the semiconductor-semiconductor transition (II to III), as may also be seen in Fig. 1. There is no apparent variation in the coordination number at the semiconductor-metal transition.

Most of the observations can be understood as follows. When Te is added to Se it enters in the main as a substitutional impurity into the Se chains. This is required by the observation[11] that the coordination remains twofold for $x > 0.4$. There must be nevertheless a substantial number of defects,[16] in particular, C_3^+ (a threefold-coordinated chalcogen cation). The Fermi level is then pinned at this level, in the alloy. Mott and Davis[2] show that, as a consequence, the activation energy for conduction is reduced by $\frac{1}{3}$. This is consistent with the 1.2-eV activation energy in pure Se and the 0.8-eV activation in the Se-rich alloys.

However, as x drops below 0.4 two effects occur: the activation energy goes *up* again to 1.2 eV and the coordination number begins to rise above 2. It therefore appears that the semiconductor-semiconductor transition occurs when threefold-coordinated Te atoms become sufficiently abundant. It is not, however, clear why the activation energy should rise in these circumstances. The final semiconductor-metal transition, II→III, does not seem to be associated with any structural change, despite the minimum[14] in α. It is probable that the Fermi level simply moves into the conduction band.

Cutler and Bez[17] have described these alloys in terms of a bond equilibrium model. They consider mainly the range $0.3 < x < 1.0$. Starting from pure Se, they compute the development of Se—Te bonds as Te is added and also the formation of defects. There are two major effects from the present viewpoint. One is the narrowing of the gap as Se—Te and Te—Te bonds replace the stronger Se—Se bonds. The other is the generation of gap states by the formation of defects. The defects considered are those introduced by Street and Mott[16(a)] and by Kastner *et al.*[16(b)] for glassy chalcogenides. In particular, singly bound chalcogens C_1^0 and C_1^- (using the notation of Kastner *et al.*[16(b)]) and threefold-coordinated C_3^+ are used. It is the C_1^0, for example, which is responsible for the spin susceptibility. The C_3^0 center is also paramagnetic but much less numerous than the C_1^-. Tsuchiya and Seymour[15] have suggested a description based on a inhomogeneous structure model.

We have measured the normal reflectance of a series of molten Se_xTe_{1-x} alloys. The optical data support the general view of the alloy system given above.

II. EXPERIMENTAL

A. Apparatus description

An experimental apparatus was designed to compare simultaneously the measured reflected intensity of a liquid sample with a known reference. The selected reference consists of a back surface Al mirror evaporated onto sapphire.

The design as shown in Fig. 2, consists of two light sources, a quartz-halogen lamp *H* and a deuterium lamp *D*. Their beams are combined at *BC* and then focused with a quartz lens *L*. The light is divided at *BD* into two equally intense beams. These beams are then sent vertically up by two mirrors *SM* and *RM* equidistant from *BD*. Before arriving at the sample and reference, each beam is chopped at ~50 Hz with a 90° phase difference between them. The light from sample and reference is normally reflected and returns to the beam divider. The returning beam is then partially deflected with a beam splitter *BS*. The signal is detected after the beam goes through a monochromator. The signal at the detector is shown in the inset of Fig. 2. It corresponds to a sum of square waves displaced from each other by 90°. The signal is amplified and discriminated by two lock-in analyzers referenced to the light chopper frequency. The phase of the analyzers is tuned by zeroing the output when one of the beams is covered and vice versa. This makes the ouput of one analyzer directly proportional to the sample reflected intensity. The output of the other analyzer is directly proprotional to the reference reflected intensity.

The sample sits in a furnace controlled with a Chromel-Alumel thermocouple. The temperature of the sample is controlled within ±5 °C. The sample is encapsulated in a sapphire tube with a flat sapphire window at the bottom through which the reflectance is measured. The tube is sealed at the oth-

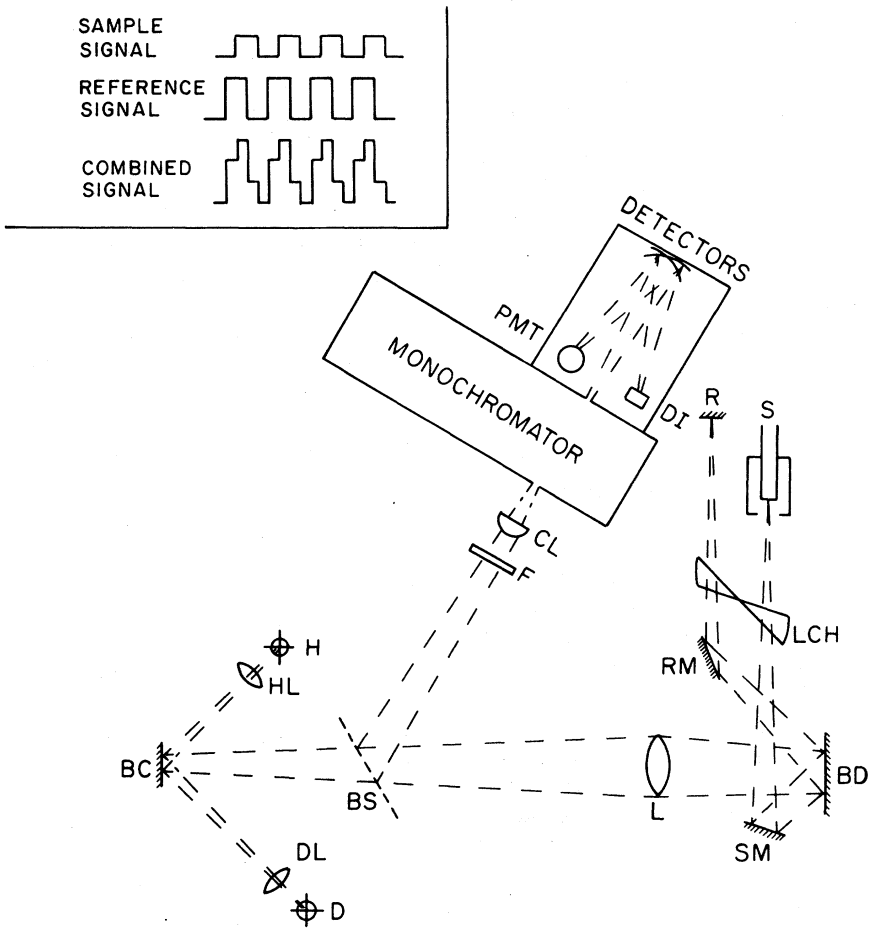

FIG. 2. Schematic of the optical apparatus. The drawing is not to scale. *H*, halogen lamp; *D*, deuterium lamp; *HL*, *DL*, and *L*, convergent quartz lenses; *BC*, beam combiner; *BS*, beam splitter, *BD*, beam divider; *SM* and *RM*, mirrors; *LCH*, light chopper; *R*, reference reflector; *S*, sample; *F*, filter; *CL*, cylindrical lens; *PMT*, photomultiplier tube; and *DI*, Si and Pb-S diodes. The inset displays the waveform of the electrical output of the detectors.

er end with a stopcock through a Pyrex taper joint. The Pyrex is attached to the sapphire with a low vapor pressure epoxy. This part of the cell remains outside the furnace and is thermally isolated with a boron nitride jacket.

B. Sample preparation

The cells were ultrasonically cleaned in a NH_3-based detergent solution for 30 min. They were rinsed and soaked in boiling deionized, distilled H_2O for 1 h. Then they were rinsed in isopropanol before being dried with hot air. The final drying step was done in a vacuum chamber connected to a He-filled glove box. The cells were placed on the vacuum chamber which was pumped to pressures $\sim 10^{-6}$ Torr for 2 h. The samples were prepared in a He-filled glove box. After loading, the cells were evacuated and filled with He to a pressure of 200 Torr at room temperature. Samples were prepared from 99.999% pure Se and 99.999% pure Te. Both materials were sealed in evacuated quartz ampules and heated to about 600 °C and 700 °C, respectively, for 12 h before being mixed.[9]

Concentrations were accurate to 1%. The concentration of the sample was varied by reintroducing the cell into the He glove box and adding the appropriate component.[18] The volume of the sample was always kept under 0.30 cm^3 so as to assure a uniform composition. The samples were heated and agitated after melting, before the data were collected.

C. Data analysis

The data gathered from the apparatus consists of the detected intensity of the light reflected by the

sample and by reference behind sapphire for a given energy. The ratio, R_m, of these two intensities is then computed; that is, the ratio of the sample reflectance intensity behind the sapphire to the reference reflectance intensity behind the sapphire. In order to obtain the absolute reflectance of the sample-sapphire interface R_i the ratios R_m were separated with the use of the following equation[19,20]:

$$R_i=\left[R_m\left[\frac{r^2+|r^2|}{1+r|r|^2}-r^2\right]\right]\Big/\left[1-R_m r^2\left[\frac{r^2+|r|^2}{1+r^2|\hat{r}|^2}\right]\right], \tag{1}$$

where

$$r=(n_a-n_s)/(n_a+n_s), \tag{2}$$

with $n_a=1.0$, the air index of refraction; with n_s, the sapphire index of refraction[21–24] (for a given energy); and with $|r|^2$, the Al reflectance[25–27] (for a given energy). Interference effects were neglected since the slits of the monochromator were 1.0 mm wide.

A Kramers-Kronig analysis is the standard technique to follow in analyzing optical data. However, the fact that these reflectance data range in energy only from 0.7 to 5.5 eV does not justify the use of this technique. Instead, an alternative method was used. This technique, which we have used in the past,[18] consists of an iterative procedure for adjusting the parameters of a model for the optical joint density of states (OJDS) to fit the reflectance data.[28] The approach is based on the relation between the imaginary part of the dielectric constant and the OJDS as derived by Mott[2] and others[29–31]:

$$\epsilon_2(\omega)=2\left[\frac{2\pi e}{m\omega}\right]^2\Omega|M|^2 \times\int_{E_f-\hbar\omega}^{E_f}d\varepsilon\, g_f(\varepsilon)g_i(\varepsilon-\hbar\omega), \tag{3}$$

where g_i and g_f are the densities of states of the initial and final states, respectively, M is the transition matrix element which is assumed energy independent, and Ω is the cell volume.

The integration was done taking into account four contributions to ϵ_2, namely, transitions from

$$g_v(\varepsilon-\hbar\alpha) \text{ to } g_v(\varepsilon),$$

transitions from

$$g_c(\varepsilon-\hbar\omega) \text{ to } g_c(\varepsilon), \tag{4}$$

transitions from

$$g_v(\varepsilon-\hbar\omega) \text{ to } g_c(\varepsilon),$$

and transitions from

$$g_c(\varepsilon-\hbar\omega) \text{ to } g_v(\varepsilon),$$

where g_v and g_c are, respectively, valence- and conduction-band densities of states. This takes into consideration both inter- and intraband effects.

The model selected for the OJDS consists of two Gaussians. The first $g_v(\varepsilon)$ is centered at the origin with an amplitude Z_1 and a width determined by A_1. The second Gaussian $g_c(\varepsilon)$ is centered at $2E_f$, has an amplitude Z_2, and a width determined by A_2. We have the following:

$$g_v(\varepsilon)=Z_1\exp(-A_1\varepsilon^2) \tag{5}$$

and

$$g_c(\varepsilon)=Z_2\exp[-A_2(\varepsilon-2E_f)^2]. \tag{6}$$

The model has five parameters to be adjusted, namely, Z_1, A_1, A_2, A_2, and E_f. With the aid of the Kramers-Kronig dispersion relations[32,33] $\epsilon_1(\omega)$ was evaluated from $\epsilon_2(\omega)$ to be

$$\epsilon_1(\omega)=1+\frac{\epsilon_2(\omega)}{\pi}\left[\ln\left[\frac{E_{\max}-\hbar\omega}{E_{\max}+\hbar\omega}\right]-\ln\left[\frac{\hbar\omega-E_{\min}}{\hbar\omega+E_{\min}}\right]\right] +\frac{2}{\pi}\mathcal{P}\int_{E_{\min}}^{E_{\max}}dx\frac{\epsilon_2(x)-\omega\epsilon_2(\omega)}{x^2-\omega^2}, \tag{7}$$

where $\mathcal{P}$ refers to the principal value and $E_{\max}$ and $E_{\min}$ are upper and lower energy bounds, set to make the numerical integration possible. A simplex technique was used to minimize Δ^2, where

$$\Delta^2=\sum[R_c(\hbar\omega)-R_i(\hbar\omega)]^2. \tag{8}$$

In Eq. (8), R_c is the calculated reflectance of the sample-sapphire interface and is given by[19]

$$R_c(\omega)=\frac{[(n_s-n)-ik][(n_s-n)+ik]}{[(n_s+n)-ik][(n_s+n)+ik]}, \tag{9}$$

where n is the sample index of refraction as calculated from Eqs. (3) and (7) and k is the sample extinction coefficient.

III. RESULTS

The experiment measures the relative reflectance behind sapphire with a precision of 0.1%. Prelimi-

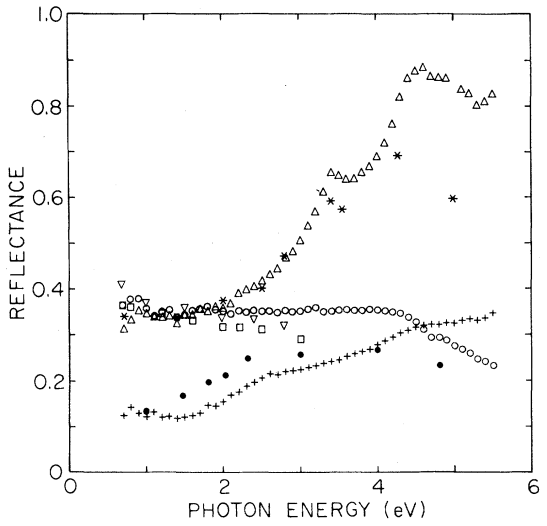

FIG. 3. Reflectances of different samples. ○, liquid Te at 500 °C in contact with a sapphire window; □, Te (Ref. 37); ∇, Te (Ref. 9); +, amorphous Se at 27 °C in contact with a sapphire window; ●, Se (Refs. 35 and 36); Δ, crystalline Si at 27 °C; *, Si (Ref. 34).

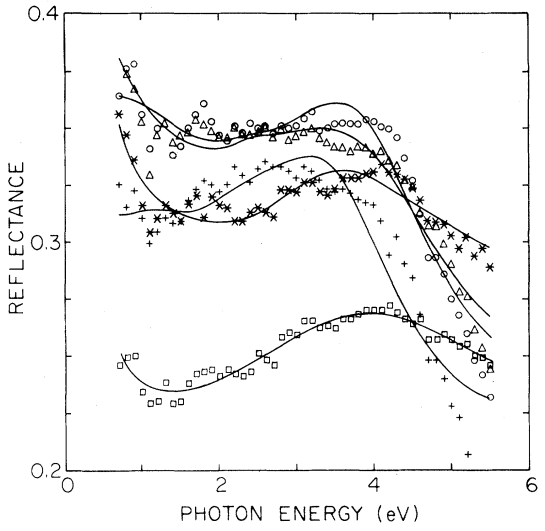

FIG. 4. Reflectance of liquid Se_xTe_{1-x} alloys at 500 °C in contact with a sapphire window. Full curves are fits to the data. ○, $x=0.0$; +, $x=0.1$; △, $x=0.2$; *, $x=0.3$; □, $x=0.4$.

nary tests were made by measuring the reflectance of known materials. Silicon,[34] amorphous selenium,[35,36] and liquid tellurium[9,37] were used for the tests shown in Fig. 3. The results obtained agree within 5% with the reported values in an energy range of 0.7 to 4.0 eV. Beyond that range discrepancies seem to increase, with measured reflectances being consistently above the literature values. Absolute reflectances are reproducible within 1% for energies below 4.0 eV and within 5% for energies above. Discrepancies are produced by changes in the alignment and changes in the reference mirror. Deficiencies in the reference mirror coating as well as deterioration with time make the reference reflectance different from the values reported in the literature. As a consequence errors are introduced in the calculation of the absolute reflectance. Two types of measurements were made: a concentration scan and a temperature scan.

A. Concentration scan

Measurements were made at 500 °C for 11 different concentrations including both pure Se and pure Te. The concentration scan was done on steps of 10 at. % Se. The absolute reflectance behind a sapphire window is shown in Figs. 4–6. The data, as expected, show no dominant structural features. The curves show a continuous decrease in the overall reflectance as the Se concentration is increased. Te-rich alloys show metallic behavior while Se-rich alloys show a semiconducting one. All curves display a sharp drop from 0.7 to 1.0 eV.

For the $x<0.3$ samples, reflectance is a decreasing function of photon energy with almost zero slope in the midrange of the $x=0.2$ sample. For the rest of the samples the reflectance is an increasing function of the photon energy for $\hbar\omega > 1.0$ eV.

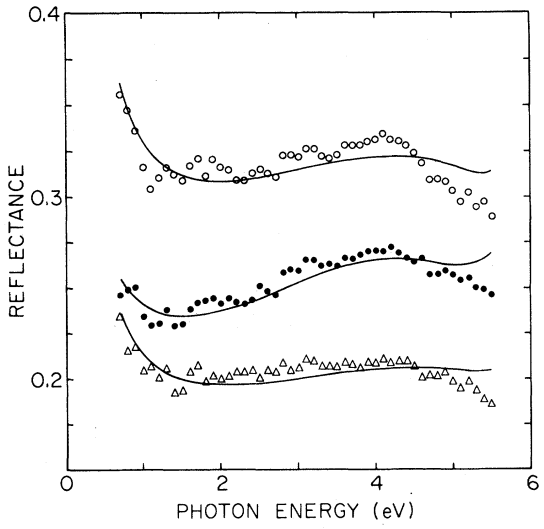

FIG. 5. Reflectance of liquid Se_xTe_{1-x} alloys at 500 °C in contact with a sapphire window. Full curves are fits to the data. ○, $x=0.3$; ●, $x=0.4$; △, $x=0.5$.

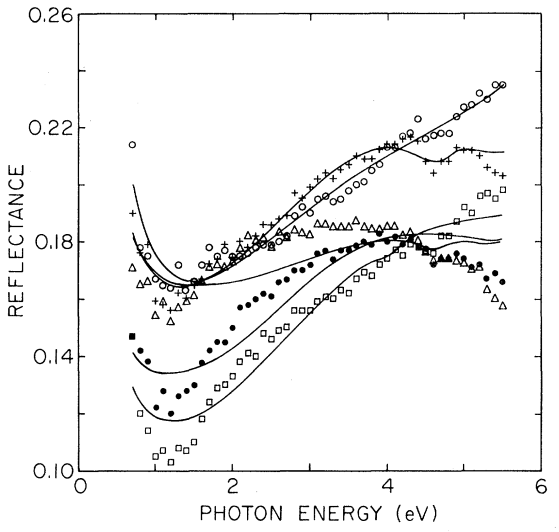

FIG. 6. Reflectance of liquid Se_xTe_{1-x} alloys at 500 °C in contact with a sapphire window. Full curves are fits to the data. ○, $x=0.6$; +, $x=0.7$; △, $x=0.8$; ●, $x=0.9$; □, $x=1.0$.

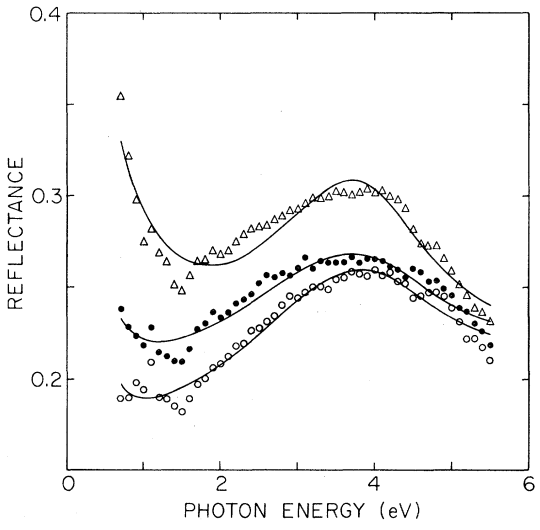

FIG. 7. Reflectance of liquid $Se_{0.4}Te_{0.6}$ in contact with a sapphire window at different temperatures. Full curves are fits to the data. △, $T=600$ °C; ●, $T=500$ °C; ○, $T=400$ °C.

The reflectance drops distinctly as the concentration changes from $x=0.3$ to 0.4. There is very little concentration dependence in the range of 0.70 to 3.0 eV for the samples with $0.5<x<0.9$. However, there is a drop on the reflectance on going from $x=0.8$ to $x=0.9$ to $x=1.0$. Slopes are generally steeper in the Se-rich samples. Three different regimes can be discerned. One is the range $x<0.3$, where R is a decreasing function of $\hbar\omega$. The second is the range $0.4<x<0.8$, where the magnitude of the reflectance changes little and R increases somewhat with $\hbar\omega$. Finally, for $0.8<x<1.0$ there is a further drop in R and the dependence on photon energy steepens somewhat.

B. Temperature scan

Measurements were made on the $x=0.4$ alloy at three different temperatures: 400 °C, 500 °C, and 600 °C. This time the cell was filled with He to a pressure of 150 Torr at room temperature to avoid pressures above 1 atm on the 600 °C run. The cell was placed on the apparatus and the three runs were made without repositioning. The sequence of the runs was first 500 °C, then 400 °C, and finally 600 °C, to avoid propagation of systematic errors. The resulting curves are shown in Fig. 7. The reflectance decreases as the temperature is decreased. This is especially noticeable in the infrared region. The high-temperature curve shows a tendency toward metallic behavior similar to the Te-rich data. The low-temperature curve shows a tendency toward semiconducting behavior somewhat similar to the Se-rich alloys. It is interesting to note that the concentration scan effects can be in a sense reproduced by a temperature scan. This suggest two ways to achieve the same transition on this particular system, as also indicated by Fig. 1. Acknowledgment is made to the fact that the $x=0.4$ data in Fig. 5 and the 500 °C data in Fig. 7 do not perfectly agree. The data correspond to two different samples under the same conditions. The discrepancies are attributed to slight changes of alignment, introduced while positioning the samples and, as previously mentioned, deterioration of the reference mirror with time.

IV. ANALYSIS

The values of the five parameters of the model OJDS of Eqs. (5) and (6) were varied until the computed reflectance matched the measured one. Figures 4–7 show the measured reflectances together with the reflectances calculated using the parameters given in Table I. The agreement is generally within 0.2% per point and may be regarded as excellent.

The fitting procedure began with the Te reflectance. The parameters obtained for the Te data were used as starting parameters in the interative fitting routine for the $x=0.1$ data. The final parameters for the $x=0.1$ data were used to start the process for the $x=0.2$ data and so on. A sudden jump in the trend of the parameters with x occurred at the

TABLE I. Parameters of the model OJDS that provide the best fit to the experimental data. The parameters are separated into groups with the different regimes discussed in the text.

x	Temperature (°C)	Z_1 (arbitrary units)	A_2 (eV^{-2})	Z_2 (arbitrary units)	A_2 (eV^{-2})	E_f (eV)	%Δ per point
0.0	500	31	0.15	1 600	2.30	1.04	0.140
0.1	500	25	0.25	1 600	2.10	1.04	0.214
0.2	500	39	0.10	1 100	1.70	1.05	0.122
0.3	500	32	0.02	1 200	0.80	1.55	0.087
0.4	500	63	0.09	550	1.10	1.30	0.052
0.3	500	5 700	13.00	16 000	0.13	5.75	0.136
0.4	500	2 400	7.50	19 000	0.16	5.37	0.099
0.5	500	5 700	14.00	11 000	0.12	5.93	0.093
0.6	500	130	0.84	4 800	0.24	3.87	0.067
0.7	500	1 600	20.00	13 000	0.21	4.75	0.058
0.8	500	12 000	140.00	12 000	0.14	5.63	0.144
0.9	500	1 300	16.00	15 000	0.23	4.69	0.097
1.0	500	1 000	120.00	6 000	0.24	4.13	0.094
0.4	600	54	0.41	280	0.30	1.34	0.118
0.4	500	64	0.19	510	1.10	1.29	0.078
0.4	400	82	0.31	410	0.95	1.37	0.084

$x=0.5$ mixture. As a result, the order of sequence was reversed after $x=0.7$ and the $x=0.5$, 0.4, and 0.3 data fitted again. No satisfactory fits for the $x=0.2$ and smaller x data could be obtained in the descending sequence. As may be seen in Table I there are two distinct sequences of parameters: One for x increasing from 0 up to 0.4, the other starting from $x=1.0$ down to 0.3. There is also a break at $x=0.6$ in some of the parameters. The trends of the parameters as x is varied may be used to define three different regimes in the concentration diagram. In the metallic regime, $x<0.3$, there is a large overlap between the two Gaussian bands of the model. No band gap is observed in the OJDS and the density of states is large at E_f. The model valence band is broader than the conduction band ($A_1<A_2$ in Table I). At the same time the valence band has a much lower peak value ($Z_1<Z_2$ in Table I). The area under the conduction-band density-of-states curve is more than twice that of the valence band.

In the second regime, $0.2<x<0.6$, there is a gap in the OJDS. This time the conduction band is broader than the valence band ($A_1>A_2$ in Table I) as opposed to the previous regime. Once again the valence band has a much lower peak value ($Z_1<Z_2$ in Table I). The gap that appears in the OJDS is not symmetric about E_f. In fact E_f lies within the tail of the Gaussian representing the conduction band. We presume that the states of the conduction band lying below E_f are localized because the density of states is quite small there. The position of E_f in the conduction band suggests that, according to the model, interband processes are never seen in this regime. This type of behavior would make the parameters pertaining to the valence band (Z_1 and A_1) insensitive to the fitting process and this is, in fact, what has been observed.

The third regime is the Se-rich end of the composition diagram where $0.50<x$. In many respects this regime is similar to the previous one. However, E_f is somewhat smaller and optical excitations from the valence band are possible at the photon energies used. Also the valence band of the model OJDS is narrower than in the previous semiconducting regime. (This can be seen on the increment of A_1 in Table I.)

Table I gives the parameters of the model OJDS that match the reflectance of the sample-sapphire interface at the three temperatures at which the $x=0.4$ alloy was measured. The 500 °C parameters were obtained starting from the resulting parameters of the $x=0.4$ in Table I. The $T=400$ °C and 600 °C parameters were obtained starting from the resulting

parameters of the $T=500\,^{\circ}C$ data. The parameters shown at the bottom of Table I for the temperature scan follow the trends of region II, $0.2<x<0.6$, mentioned above. The $T=600\,^{\circ}C$ data fall within region II towards the metallic regime somewhat analogous to $x=0.3$ and the $T=400\,^{\circ}C$ data fall within the same region towards the region I regime somewhat analogous to $x=0.5$.

V. DISCUSSION

The optical data are entirely consistent with the description of Se_xTe_{1-x} alloys based on the dc transport parameters. That is, there are three different conduction regimes as labeled in Fig. 1. In the Se-rich regime (region I) the alloys are semiconducting with an activation energy of 0.8 eV as if the Fermi level is pinned by defects.[2] At intermediate concentrations (region II) the alloys are still semiconducting, but with a higher activation energy of 1.2 eV. Finally in region III the Te-rich alloys are metallic.

The model OJDS yields reflectances which accurately reproduce the data. As in our previous work[18] there is no way to determine whether or not the density of states in unique. However, the use of Gaussians as a model of the OJDS leads to substantially better reproduction of the experimental data. We must stress that the final parameters of the OJDS may not be unique. The use of numerical minimization to determine the model parameters is always open to the question of whether or not the minimum attained is local. In fact, we have obtained high-quality fits of the data for $x=0.4$ and $x=0.3$ data using two dramatically different densities of states (see Table I). Strictly, then, it may not be possible to regard the parameters derived from this method as representative of the alloy. Some trends may nevertheless be significant. Note first that it is certainly not necessary to postulate states in the gap in order to describe the reflectance. Only Gaussians with varying overlap have been used. We also find the gap in regime I to be systematically higher than that in regime II. While this trend is opposite to that of the conductivity activation energy it is entirely consistent with the Fermi-level pinning model of Mott and Davis.[2] The numerical values of the gap are large (2.7 and 2.5 eV, respectively) which suggests that intraband transitions are important as E_f lies near the bottom of the conduction band. The existence of dual sets of parameters providing excellent fits to the $x=0.3$ and $x=0.4$ data may be indicative of the metal-nonmetal transition in that concentration range. Strong band overlap is found, of course, in region III. Further interpretation of the model OJDS is difficult in the absence of theoretical models for these alloys.

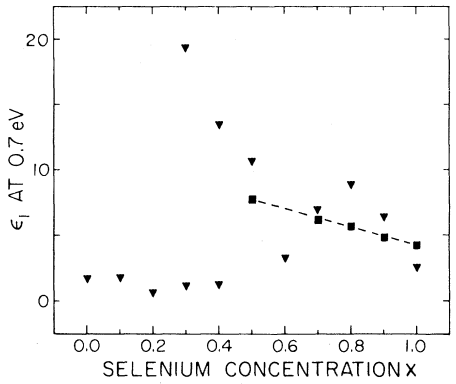

FIG. 8. Real part of the dielectric constant at 0.7 eV of liquid Se_xTe_{1-x} alloys. ▼, calculated from a model of the optical joint density of states used to fit the reflectance data; ■, calculated directly from our reflectance and Perron's (Ref. 7) optical-absorption data.

An anomaly in the real part of the dielectric constant as discussed by Cheshnovsky[38] and others[39–42] is present in many systems undergoing a metal-nonmetal (MNM) transition. We tested the theory and in our case the MNM transition occurs at $x=0.3$. We have knowledge of the low-frequency dielectric constant [$\epsilon_1(\hbar\omega=0.7$ eV)] from two approaches. The first comes from a combination of Perron's optical-absorption measurements[7] with our reflectivity data and the second is extracted from our model of the OJDS. Figure 8 displays the low-frequency ϵ_1 as a function of Se concentration. The agreement between the two approaches is not exact; however, the trends are consistent. The dielectric constant ϵ_1 increases as the MNM transition is approached from the Se-rich side, drops discontinuously at $x=0.3$, and is independent of x in the Te-rich end.

ACKNOWLEDGMENTS

This material is based upon work supported in part by the U.S. National Science Foundation under Grant No. DMR 78-21744 and in part by the R. A. Welch Foundation. One of us (R.F.) acknowledges support by Consejo Nacional de Ciencia y Tecnología of Mexico under fellowship 17348.

[1]M. Cutler, *Liquid Semiconductors* (Academic, New York, 1977).

[2]N. F. Mott and E. A. Davis, *Electronic Processes in Non-Crystalline Materials,* 2nd ed. (Clarendon, Oxford, 1979).

[3]J. C. Perron, Adv. Phys. 16, 657 (1967).

[4](a) M. Cutler and R. Fischer, J. Non-Cryst. Solids 35-36, 1289 (1980); (b) H. Rasolondramanitra and M. Cutler, Bull. Am. Phys. Soc. 27, 309 (1982).

[5]M. Yao, K. Suzuki, H. Hoshino, and H. Endo, J. Phys. (Paris) Colloq. 41, C8-28 (1980).

[6]J. A. Gardner and M. Cutler, Phys. Rev. B 20, 529 (1979).

[7](a) J. Rabit and J. C. Perron, Phys. Status Solidi B 65, 255 (1974); (b) J. Phys. (Paris) Colloq. 42, C4-1047 (1981); (c) M. Cutler (private communication).

[8]K. J. Siemsen and E. W. Fenton, Phys. Rev. 161, 632 (1967).

[9]D. M. Trotter, Jr., U. Even, and J. C. Thompson, Phys. Rev. B 17, 4004 (1978).

[10]J. Ruska, in *Proceedings of the International Conference on Amorphous and Liquid Semiconductors,* edited by J. Stuke and W. Brenig (Taylor and Franics, London, 1973), p. 779.

[11]R. Bellissent and G. Tourand, in *Condensed Matter Physics II,* edited by J. T. Devreese, L. F. Demmens, V. E. Van Daren, and J. Van Royen (Plenum, New York, 1981), p. 149.

[12]M. Hansen and K. Anderko, *Constitution of Binary Alloys,* 2nd ed. (McGraw-Hill, New York, 1958), p. 1188.

[13](a) F. Hensel, in *Amorphous and Liquid Semiconductors,* edited by W. E. Spear (University of Edinburgh, Edinburgh, 1977), p. 815; (b) A. Andreev, E. A. Lebedev, E. A. Shincerator, and L. N. Shumilova, Fiz. Tverd. Tela (Leningrad) 15, 382 (1973) [Sov. Phys.—Solid State 15, 277 (1973)].

[14]H. Radscheit, J. Phys. (Paris) Colloq. 42, C4-1063 (1981).

[15]Y. Tsuchiya and E. F. W. Seymour, J. Phys. C 15, L687 (1982).

[16](a) R. A. Street and N. F. Mott, Phys. Rev. Lett. 35, 1293 (1975); (b) M. Kastner, D. Adler, and H. Fritzsche, *ibid.* 37, 1504 (1976).

[17]M. Cutler and W. G. Bez, Phys. Rev. B 23, 6223 (1981).

[18]R. Fainchtein, U. Even, C. E. Krohn, and J. C. Thompson, J. Phys. F 12, 633 (1982).

[19]M. Born and E. Wolf, *Principles of Optics,* 5th ed. (Pergamon, New York, 1975), p. 61.

[20]W. Weinstein, Vacuum 4, 3 (1954).

[21]I. H. Malitson, J. Opt. Soc. Am. 52, 1377 (1962).

[22]E. T. Arakawa and M. W. Williams, J. Phys. Chem. Solids 29, 735 (1968).

[23]M. A. Teppesen, J. Opt. Soc. Am. 48, 629 (1958).

[24]V. Bartashonskii, M. P. Kuzyk, N. S. Pidzyrailo, I. V. Stefanskii, and K. P. Argunov, Ukr. Fiz. Zh. (Russ. Ed.) 21, 155 (1976).

[25]H. Ehrenreich, H. R. Philipp, and B. Segall, Phys. Rev. 132, 1918 (1963).

[26]G. Hais and J. E. Waylonis, J. Opt. Soc. Am. 51, 719 (1961).

[27]G. Mathewson and H. P. Myers, Phys. Scr. 4, 291 (1971).

[28]C. E. Krohn and J. C. Thompson, J. Non-Cryst. Solids 35-36, 1283 (1980).

[29]N. K. Hindley, J. Non-Cryst. Solids 5, 17 (1970).

[30]K. Hoshino, J. Phys. Soc. Jpn. 41, 1453 (1976).

[31](a) R. D. Bringans and C. M. Sutton, Solid State Commun. 19, (1976); (b) C. M. Sutton, *ibid.* 16, 327 (1975).

[32]F. Wooten, *Optical Properties of Solids* (Academic, New York, 1972), p. 173.

[33]E. A. Guillemin, *The Mathematics of Circuit Analysis* (MIT Press, Cambridge, 1949), p. 339.

[34]H. R. Philip and H. Ehrenreich, Phys. Rev. 129, 1550 (1963).

[35]J. Stuke, Z. Phys. 134, 194 (1953).

[36]A. G. Leiga, J. Opt. Soc. Am. 58, 1441 (1968).

[37]J. N. Hodgson, Philos. Mag. 8, 735 (1963).

[38]O. Cheshnovsky, U. Even, and J. Jortner, Philos. Mag. B 44, 1 (1980).

[39]Y. Imry, Y. Gefen, and D. J. Bergman, Phys. Rev. B 26, 2436 (1982).

[40]W. Hefner and F. Hensel, Phys. Rev. Lett. 48, 1682 (1982).

[41]H. F. Hess, K. DeConde, T. F. Rosenbaum, and G. A. Thomas, Phys. Rev. B 25, 5578 (1982).

[42]D. W. Mehaffey and D. A. Jerde, Rev. Mod. Phys. 40, 710 (1968).